Prediction of the dynamic behavior of a solar chimney by means of artificial neural networks

Predicción del comportamiento dinámico de una chimenea solar mediante redes neuronales artificiales

A. Tlatelpa-Becerro[1]*, R. Rico-Martínez[2], M. Cárdenas-Manríquez[2], G. Urquiza[3], F.B. Alarcón-Hernández[4], M.C. Fuentes-Albarran[4]

[1]*Escuela de Estudios Superiores de Yecapixtla-UAEM. 62820, Morelos, México.*
[2]*Tecnológico Nacional de México-Instituto Tecnológico de Celaya. 38000, Guanajuato, México.*
[3]*Centro de Investigación en Ingeniería y Ciencias Aplicadas-UAEM. 62209, Morelos, México.*
[4]*Escuela de Estudios Superiores de Xalostoc-UAEM. 62717, Morelos, México.*

Abstract

A strategy is described for the construction of a reference model for the design of solar chimneys that includes variations in geometry and materials of the chimney's components. The model will be developed from dynamic simulations in the transient state of the solar chimney under solar irradiation real conditions. The strategy is based on the artificial neural networks (ANNs) generalization properties allowing predictions for multiple geometries and materials of the solar chimney. The strategy can serve as a basis for cost optimization during the design stage by allowing selection of the best geometry and materials given the desired performance specification for the solar chimney, including operating and replacement costs.
Keywords: Artificial neural networks, mathematical model, thermal comfort.

Resumen

Se describe una estrategia para la construcción de un modelo de referencia para el diseño de chimeneas solares que incluye variaciones en la geometría y materiales de los componentes de la chimenea. El modelo se desarrolla a partir de simulaciones dinámicas en el estado transitorio de la chimenea solar en condiciones reales de irradiación solar. La estrategia se basa en las propiedades de generalización de las redes neuronales artificiales (ANN) que permiten predicciones para múltiples geometrías y materiales de la chimenea solar. La estrategia puede servir como base para la optimización de costos durante la etapa de diseño al permitir la selección de la mejor geometría y materiales dada la especificación de desempeño deseada para la chimenea solar, incluidos los costos de operación y reemplazo.
Palabras clave: Redes neuronales artificiales, Modelo matemático, Confort térmico.

1   Introduction

A solar chimney is a ventilated cavity that uses solar energy to improve natural ventilation. For the last three decades, these systems have been used in architectural settings to decrease the energy used by mechanical methods. They are increasingly being incorporated into new housing designs to provide natural ventilation under bioclimatic approaches, mainly in hot climates. Generally, they are a glass cover, a cavity for flow passage, and a metal plate that absorbs solar energy.

Thus, Solar Chimneys are systems that improve energy efficiency and thermal comfort. To design, it is necessary to estimate the mass flow rates and temperatures based on the characteristics of the chimney. This analysis has been executed mainly through stationary -state simulations (Patel *et al.*, 2014; Amori and Saif, 2012), looking for the geometry that will give the maximum heat transfer as a function of the mass flows. Likewise, the effect of incident solar radiation on inclined chimneys has been studied (Imran, *et al.*, 2015), looking at an optimal angle as part of the best design. As part of the design strategies, the combination with wind towers has been studied (Bansal, *et al.*, 1994), as well as computational fluid dynamics approaches for two-dimensional analysis on the dynamic behavior of chimneys to cool small rooms (Layeni *et al.* al., 2020; Wenguang *et al.*, 2020; Khedari *et al.*, 1999). Mathematical models in a transitory state have also been reported to predict the behavior of the chimney (Zhongbao and Su, 2012; Saifi *et al.*, 2012; Shi and Zhang, 2016; Sudprasert, *et al.*, 2016), analyzing the behavior of the chimney for different geometries and environmental conditions.

In this contribution, transient numerical simulations of a solar chimney are used to build an ANN reference model. The model seeks to develop a tool capable of helping in the design of the chimney, describing the effect of the geometry and the materials used in a compact and precise way and simulating its dynamics. The example involves a solar chimney with two metal plates placed in the center between two glass covers that form three cavities for airflow.

This strategy is proposed as an alternative to the application of simulations based on energy balances, which are the basis of the simulations for the design of the chimneys until now. In general, this alternative becomes unfeasible when a large number of options are studied in the geometric configuration and the materials used in the construction of the chimney due to the resulting high computational cost. Artificial Neural Networks (ANN) have proven to be a good option for the prediction of complex system behavior, including applications that involve decision making, pattern recognition, and system identification (González *et al.*, 1998; Krischer *et al.*, 1993) and control (Díaz *et al.*, 2001). These applications include studies of systems thermal behavior in mechanical engineering via systems identification that includes parametric dependence. For example, ANNs have been used for heat transfer predictions (Xie *et al.*, 2007; Islamoglu, 2003; Gongnan *et al.*, 2009; Hao and Ling 2009; Jian and Haghighat 2010), description of coiled helical tubes exchangers behavior (Reza and Rahimi, 2012) and heat pump systems (Esen and Inalli, 2009). Furthermore, ANNs have been applied in membrane energy exchanger dynamics to predict transient performance and estimate heat transfer in oscillating annular flux (Akbari, *et al.*, 2012; Akdag *et al.*, 2009). Even the ANNs have been involved in other engineering areas obtaining good results, for example: estimating the concentration of esters in the transesterification of soybean oil to produce biodiesel (Diaz, *et al.*, 2013). Predict temperatures in geothermal wells in studies geothermometry, to name a few (Brusamarello, *et al.*, 2020).

2   Solar chimney

Solar Chimneys are considered innovative technology. This innovation combines bioclimatic principles and traditional design strategies to create successful new design solutions. The operational focus of the systems is to capture solar radiation. The energy received increases the air temperature inside the Chimneys to allow hot air to rise by convection and escape outside.

Figure 1 a) shows a solar chimney located at the highest and sunniest part of a building. The Chimneys receives and takes advantage of the maximum solar radiation throughout the day. The system has two vertical metal plates, (P_{m1} and P_{m2}), located in the center between two glass covers, (G_{c1} and G_{c2}), which form three airflow cavities (C_{t1},C_{t2},and C_{t3}), see Figure 1 b).
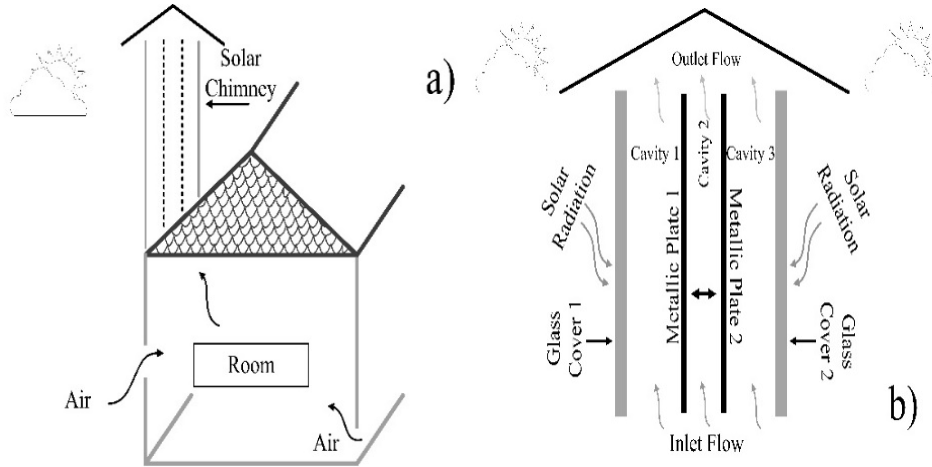
FIGURE 1. Solar Chimneys. a) Location of the chimney at the highest part of the building. b) Schematic diagram of the solar chimney.
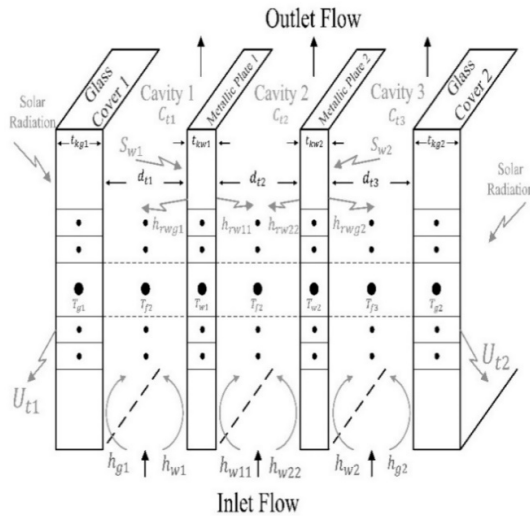

FIGURE 2. Thermal parameters in the physical model. The temperatures of each element are represented by: $T_{g1}, T_{f1}, T_{w1}, T_{f2}, T_{w2}, T_{f3}, T_{g2}$.
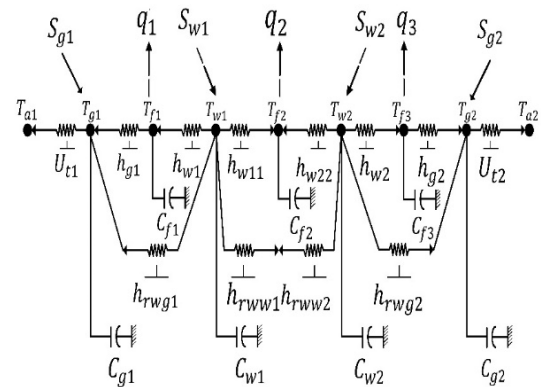

FIGURE 3. Thermal-electrical analogy of the mathematical model of the solar chimney. Each temperature element corresponds to a node to which the energy balance applies.

2.1 Physical model

The solar chimney works as follows: received solar radiation (S_{g1} and S_{g2}) on glass covers (G_{c1}, and G_{c2}) experiments transmission, reflection, and absorption. The metal plate absorbs most of the transmitted energy (S_{w1} and S_{w2}) to increase air flow and internal energy (q_1, q_2, and q_3), thus eliminating a thermal load. The heat flux implies a radiative contribution (h_{rwg1}, h_{rwg2}), and convective (h_{w1}, h_{w2}, h_{g1}, h_{g2}) through interaction with internal cavities C_{t1} and C_{t3}.

While in the cavity C_{t2} there are radiative exchanges (h_{rww1}, h_{rww2}), and convective (h_{w11}, h_{w22}) between plates, glass covers reduce convective losses (h_{wind}) and irradiance (h_{rs}), as shown in Figure 2.

2.2 Mathematical model

In thermal engineering, the heat transfer problems analysis using an electrical analogy reduces the complexity of the system. The physical model of the solar chimney in Figure 2 that describes all the convective and radiative heat transfer coefficients, airflow irradiances, and temperatures that interact in the system is used to represent the analogy in a thermal network.

Figure 3 shows the analogous form to resistive electrical circuits.

The mathematical model results from the application of the global energy balance to the thermal network, applying the 1st Law of Thermodynamics (Cengel and Boles, 2015) that shows the conservation of energy (Equation 1), under the following assumptions:

$$\dot{E}_{in} + \dot{E}_g - \dot{E}_{out} = \dot{E}_{st} \tag{1}$$

1. Natural convection throughout the system.

2. One-dimensional heat transfer for all processes through glass covers, metal plates, and airflow in each cavity.

3. The thickness of the chimney elements is considered insignificant for energy storage, and their temperature only depends on the axial dimension.

4. Air temperature only changes in the flow direction.

5. The air temperature at the inlet of each channel is the same as the ambient temperature.

6. All thermophysical properties are calculated at a mean temperature.

7. The optical and physical properties of the material (glass cover and metal plates) are temperature independent.

8. There is no power generation in the system.

Where $\dot{E}_g$ is thermal energy generation, $\dot{E}_{st}$ is the stored thermal and mechanical energy. For thermal and mechanical energy transportation through control surfaces; that is, the input and output terms are: $\dot{E}_{in}$ y $\dot{E}_{out}$.

Below are the energy equations for each element of the solar Chimneys:

Glass cover equation, G_{c1}:

$$S_{g1} + U_{t1}T_a1 + \frac{\rho_{g1}C_{g1}t_{kg1}T_{g1,i}^k}{\Delta t}$$
$$= \left(\frac{\rho_{g1}C_{g1}t_{kg1}}{\Delta t} + h_{g1,i} + h_{rwg1,i} + U_{t1}\right)T_{g1,i}^{k+1} - h_{g1,i}T_{f1,i}^{k+1}$$
$$- h_{rwg1,i}T_{w1,i}^{k+1} \tag{2}$$

Cavity air flow equation, C_{t1}:

$$M_1T_{fI1,i} + \frac{\rho_{f1}C_{f1}d_{t1}T_{f1,i}^k}{\Delta t} + h_{w1,i}T_{w1,i}^{k+1} \tag{3}$$
$$= -h_{g1,i}T_{g1,i}^{k+1} + \left(\frac{\rho_{f1}C_{f1}d_{t1}}{\Delta t} + h_{g1,i} + h_{w1,i} + M_1\right)T_{f1,i}^{k+1}$$

Metal plate equation, P_{m1}:

$$S_{w1} + \frac{\rho_{w1}C_{w1}t_{kw1}T_{w1,i}^k}{\Delta t} = -h_{rwg1,i}T_{g1,i}^{k+1}$$
$$- h_{w1,i}T_{f1,i}^{k+1}\left(\frac{\rho_{w1}C_{w1}t_{kw1}}{\Delta t} + h_{w1,i} + h_{w11,i} + h_{rwg1,i}\right.$$
$$\left. + h_{rww1,i} + h_{rww2,i}\right)T_{w1,i}^{k+1} - h_{w11,i}T_{f2,i}^{k+1}$$
$$- (h_{rww1,i} + h_{rww2,i})T_{w2,i}^{k+1} \tag{4}$$

Cavity air flow equation, C_{t2}:

$$M_2T_{fI2,i} + \frac{\rho_{f2}C_{f2}d_{t2}T_{f2,i}^k}{\Delta t} = -h_{w11,i}T_{w1,i}^{k+1} \tag{5}$$
$$+ \left(\frac{\rho_{f2}C_{f2}d_{t2}}{\Delta t} + h_{w11,i} + h_{w22,i} + M_1\right)T_{f2,i}^{k+1} - h_{w22,i}T_{w2,i}^{k+1}$$

Metal plate equation, P_{m2}:

$$S_{w2} + \frac{\rho_{w2}C_{w2}t_{kw2}T_{w2,i}^k}{\Delta t} = -(h_{rww1,i} + h_{rww2,i})T_{w1,i}^{k+1}$$
$$- h_{w22,i}T_{f2,i}^{k+1}\left(\frac{\rho_{w2}C_{w2}t_{kw2}}{\Delta t} + h_{w2,i} + h_{w22,i} + h_{rwg2,i}\right.$$
$$\left. + h_{rww1,i} + h_{rww2,i}\right)T_{w2,i}^{k+1} - h_{w2,i}T_{f3,i}^{k+1} - h_{rwg2,i}T_{g2,i}^{k+1} \tag{6}$$

Cavity air flow equation, C_{t3}:

$$M_3T_{fI3,i} + \frac{\rho_{f3}C_{f3}d_{t3}T_{f3,i}^k}{\Delta t} = -h_{w2,i}T_{w2,i}^{k+1} \tag{7}$$
$$+ \left(\frac{\rho_{f3}C_{f3}d_{t3}}{\Delta t} + h_{w2,i} + h_{g2,i} + M_3\right)T_{f3,i}^{k+1} - h_{g2,i}T_{g2,i}^{k+1}$$

Glass cover equation, G_{c2}:

$$S_{g2} + U_{t2}T_{a2} + \frac{\rho_{g2}C_{g2}t_{kg2}T_{g2,i}^k}{\Delta t} = -h_{rwg2,i}T_{w2,i}^{k+1} \tag{8}$$
$$- h_{g2,i}T_{f3,i}^{k+1}\left(\frac{\rho_{g2}C_{g2}t_{kg2}}{\Delta t} + h_{g2,i} + h_{rwg2,i} + U_{t2}\right)T_{g2,i}^{k+1}$$

Equations 2 - 8 are represented in a matrix arrangement, where the temperatures of each element of the chimney is the solution vector, as represented by:

$$
\begin{bmatrix}
\frac{\rho_{g1}Cp_{g1}e_{g1}T^{k}_{g1,i}tk_{g1}}{\Delta t} + U_{t1}T_{a1} + S_{g1}M_{1}T_{fI1,i} \\
+ \frac{\rho_{f1}Cp_{f1}d_{t1}T^{k}_{f1,i}}{\Delta t}S_{w1} + \frac{\rho_{w1}Cp_{w1}tk_{w1}T^{k}_{w1,i}}{\Delta t} \\
M_{2}T_{fI2,i} + \frac{\rho_{f2}Cp_{f2}d_{t2}T^{k}_{f2,i}}{\Delta t} \\
S_{w2} + \frac{\rho_{w2}Cp_{w2}tk_{w2}T^{k}_{w2,i}}{\Delta t} \\
M_{3}T_{fI3,i} + \frac{\rho_{f3}Cp_{f3}d_{t3}T^{k}_{f3,i}}{\Delta t} \\
S_{g2} + U_{t2}T_{a2} + \frac{\rho_{g2}Cp_{g2}tk_{g2}T^{k}_{g2,i}}{\Delta t}
\end{bmatrix}
=
\begin{bmatrix}
T^{k+1}_{g1,i} \\
T^{k+1}_{f1,i} \\
T^{k+1}_{w1,i} \\
T^{k+1}_{f2,i} \\
T^{k+1}_{w2,i} \\
T^{k+1}_{f3,i} \\
T^{k+1}_{g2,i}
\end{bmatrix}
\begin{bmatrix}
A_{11} & -h_{g1,i} & -h_{rwg1,i} \\
-h_{g1,i} & A_{22} & -h_{w1,i} \\
-h_{rwg1,i} & -h_{w1,i} & A_{33} & -h_{w11,i} & -A_{35} \\
 & & -h_{w11,i} & A_{44} & -h_{w22,i} \\
 & & A_{53} & -h_{w22,i} & A_{55} & -h_{w2,i} & h_{rwg2,i} \\
 & & & & -h_{w2,i} & A_{66} & -h_{g2,i} \\
 & & & & -h_{rwg2,i} & -h_{g2,i} & A_{77}
\end{bmatrix}
$$

$$(9)$$

Where, all coefficients A in the matrix are:

$$\frac{\rho_{g1}Cp_{g1}tk_{g1}}{\Delta t} + h_{g1,i} + h_{rwg1,i} + U_{t1} \qquad (A_{11})$$

$$\frac{\rho_{f1}Cp_{f1}d_{t1}}{\Delta t} + h_{g1,i} + h_{w1,i} + M_{1} \qquad (A_{22})$$

$$\frac{\rho_{w1}Cp_{w1}tk_{w1}}{\Delta t} + h_{w1,i} + h_{w11,i} + h_{rwg1,i} + h_{rww1,i} + h_{rww2,i}$$
$$(A_{33})$$

$$\frac{\rho_{f2}Cp_{f2}d_{t2}}{\Delta t} + h_{w11,i} + h_{w22,i} + M_{2} \qquad (A_{44})$$

$$\frac{\rho_{w2}Cp_{w2}tk_{w2}}{\Delta t} + h_{w2,i} + h_{w22,i} + h_{rwg2,i} + h_{rww1,i} + h_{rww2,i}$$
$$(A_{55})$$

$$\frac{\rho_{f3}Cp_{f3}d_{t3}}{\Delta t} + h_{w2,i} + h_{g2,i} + M_{3} \qquad (A_{66})$$

$$\frac{\rho_{g2}Cp_{g2}tk_{g2}}{\Delta t} + h_{g2,i} + h_{rwg2,i} + U_{t2} \qquad (A_{77})$$

$$h_{rww1,i} + h_{rww2,i} \qquad (A_{53})$$

$$h_{rww1,i} + h_{rww2,i} \qquad (A_{35})$$

Heat transfer coefficients and material property calculations are described in the following subsections.

2.2.1 Heat transfer from the glass cover to the environment

The radiation heat transfer coefficient of the glass cover ($h_{rs1,2}$) (Duffie *et al.*, 1985) and the sky temperature (T_{sky}), are evaluated by the following equations:

$$h_{rs1,2} = \frac{\sigma\varepsilon_{g1,2}(T_{g1,2} + T_{sky})(T^{2}_{g1,2} + T^{2}_{sky})(T_{g1.2} - T_{sky})}{(T_{g1,2} + T_{a1,2})}$$
$$(10)$$

$$T_{sky} = 0.0552T^{3/2}_{a1,2} \qquad (11)$$

The overall convective heat transfer coefficient of the glass cover ($U_{t1,2}$) and the coefficient of heat loss due to convection of air ($h_{wind1,2}$), are evaluated as follows by Equations 12 and 13 (Duffie *et al.*, 1985):

$$U_{t1,2} = h_{wind1,2} + h_{rs1,2} \qquad (12)$$

$$h_{wind1,2} = 5.7 + 3.8V \qquad (13)$$

2.2.2 Heat transfer between metal plates and, glass cover and metal plate

Radiation heat transfer coefficient between metal plates ($h_{rww1,2}$), and between the metal plate and the glass cover ($h_{rwg1,2}$).

$$h_{rww1,2} = \frac{\sigma(T^{2}_{w1} + T^{2}_{w2})(T_{w1} + T_{w2})}{\left(\frac{1}{\varepsilon_{w1}} + \frac{1}{\varepsilon_{w2}} - 1\right)} \qquad (14)$$

$$h_{rwg1,2} = \frac{\sigma(T^{2}_{g1,2} + T^{2}_{w1,2})(T_{g1,2} + T_{w1,2})}{\left(\frac{1}{\varepsilon_{g1,2}} + \frac{1}{\varepsilon_{w1,2}} - 1\right)} \qquad (15)$$

2.2.3 Solar Radiation

Solar irradiance absorbed by the glass cover ($S_{I1,I2}$).

$$S_{I1,I2} = \alpha S_{g1,2} \qquad (16)$$

The transmitted solar irradiance of the metal plate is evaluated by:

$$S_{w1,2} = \alpha\tau S_{g1,2} \qquad (17)$$

2.2.4 Air physical properties

The physical properties of air are evaluated at an average flow temperature for each chimney cavity. Equations 18 to 21 were obtained from data proposed by (Çengel and Boles, 2015)
Dynamic viscosity:

$$\mu_{f1,2,3} = 4 \times 10^{-8}T_{f} + 2 \times 10^{-5} \qquad (18)$$

TABLE 1. Solar chimney proposed geometries for numerical simulation.

Geometry	Length, L [m]	Depth, D_p [m]	Width, d_{t1} [m]	Width, d_{t2} [m]	Width, d_{t3} [m]
G_1	1	0.5	0.25	0.2	0.3
G_2	1.5	1	0.3	0.5	0.2
G_3	2	1.25	0.25	0.6	0.4
G_4	2.5	1.5	0.6	0.4	0.5
G_5	1.8	1.2	0.35	0.4	0.25

Density:

$$\rho_{f1,2,3} = 8 \times 10^{-6} T_f^2 - 4.2 \times 10^{-3} T_f + 1.2859 \quad (19)$$

Thermal conductivity:

$$k_{f1,2,3} = 7 \times 10^{-5} T_f + 0.0238 \quad (20)$$

Specific heat:

$$C_{f1,2,3} = 4 \times 10^{-10} T_f^5 - 2 \times 10^{-7} T_f^4 + 4 \times 10^{-5} T_f^3$$
$$- 3.3 \times 10^{-3} T_f^2 + 0.10779 T_f + 1005.7 \quad (21)$$

M is represented by the following expression:

$$M_{1,2,3} = \frac{m_{1,2,3} C_{f1,2,3}}{W \Delta x \gamma} \quad (22)$$

2.2.5 Air Mass Flow

The air mass flow rate is evaluated by Equation 23, suggested in (Bansal *et al.*, 2005):

$$m = C_d \frac{\rho_{f,o} A_0}{\sqrt{1 + A_r^2}} \sqrt{\frac{2gL(T_f - T_r)}{T_r}} \quad (23)$$

A_r, is the aspect ratio of the area and is evaluated by:

$$A_r = \frac{A_o}{A_i} \quad (24)$$

The discharge coefficient (C_d) defines the relationship between the cross-sectional area in the contracted vein and the actual opening area. Although values for different geometries have been reported in the literature (Hirunlabh *et al.*, 1999; Sakonidou *et al.*, 2008; Awbi, 1994; Ramadan and Nader, 2008; Ramadan and Nader, 2009; Chantawong, *et al.*, 2006), here the discharge coefficient (White, 2004) is evaluated for each of the proposed geometries as described in Table 1.

$$C_d = 0.5959 + 0.0312 \beta^2 .1 - 0.184 \beta^8 + 91.71 \beta^{2.5} Re_D^{-0.75} \quad (25)$$

where β is the ratio of the flow through the width ($w = d_{t1} + d_{t2} + d_{t3}$) of the chimney and the fraction that is forced to pass between each cavity (d_{t1}, d_{t2}, d_{t3}):

$$\beta = \frac{d_{t1,2,3}}{w} \quad (26)$$

The Reynolds number (Re_D) is evaluated by:

$$Re_D = \frac{\rho V D_h}{\mu} \quad (27)$$

The hydraulic diameter is calculated by:

$$D_h = \frac{2 D_p (d_{t1}, d_{t2}, d_{t3})}{(d_{t1}, d_{t2}, d_{t3}) + D_p} \quad (28)$$

The matrix system (9) is solved numerically using standard linear algebra routines.

3 Reference model

Different chimney configurations have been proposed and analyzed varying the height, depth, and width to calculate the temperatures, flows, and efficiencies of these systems (Patel *et al.*, 2014; Amori and Saif, 2012; Imran, *et al.*, 2015; Bansal, *et al.*, 1994; Layeni *et al.*, 2020; Wenguang *et al.*, 2020; Khedari *et al.*, 1999). Thus, different construction materials for chimneys can be considered, which can determine their performance by the effect of optical and physical properties. Likewise, airflow velocity, ambient temperature, and solar irradiance should be included as external parameters to describe the local conditions of the construction site. With these considerations, the behavior of the chimney is described with a numerical simulation.

The simulations are used to train an ANN reference model that describes the dynamic behavior of the chimney in a compact way. The successful construction of such a model provides an efficient and compact tool for predicting Chimneys performance

TABLE 2. Optical and physical properties of materials (Karima and Saif, 2012; Incropera and DeWitt, 1999; Oliva *et al.*, 2013).

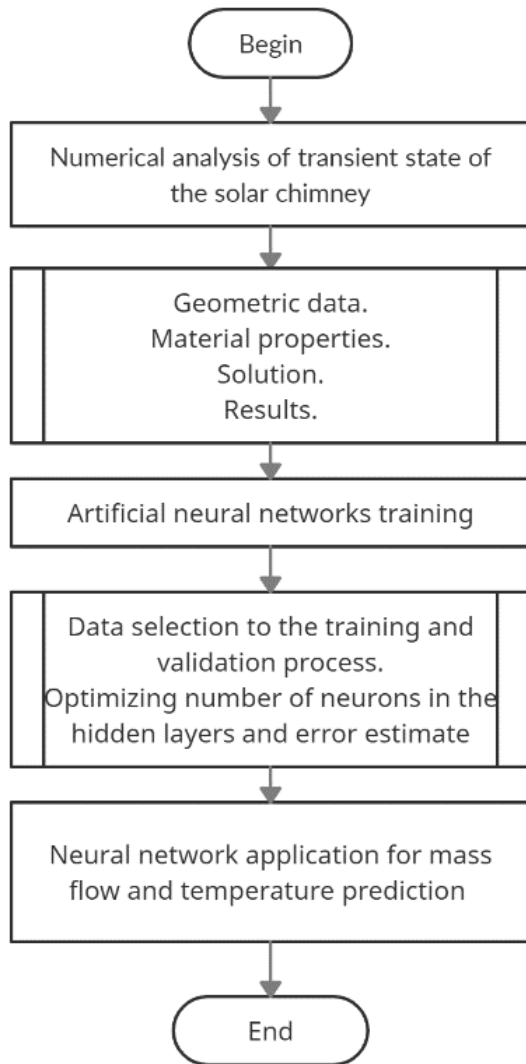| Material	ρ (kg/m^3)	Cp (J/kg °C)	Emissivity [ε]	Absorptivity [α]	Transmissivity [τ]
Ductile Steel	7850	500	0.95	0.95	——
Anodized aluminum	2720	895	0.84	0.14	——
Copper with smoke black surfaces	8950	380	0.9988	0.9988	——
Nickel Oxide	8900	450	0.49	0.79	——
Common Glass	2470	750	0.9	0.06	0.84

FIGURE 4. Flow Chart to predict the mass flow rate and the temperatures of the solar chimney elements.

at the design stage. Thus, assisting in the geometry optimization stages and the selection of suitable material.

In the following paragraphs, the construction of the ANN reference model describes the process schematically represented in the Flowchart, see Figure 4.

3.1 Transient numerical simulation parameters

The vector of temperatures in Equation 9 is calculated through computational numerical simulation. The temperatures vector corresponds to those of the glass cover (T_{g1} and T_{g2}), air (T_{f1}, T_{f2}, and T_{f3}), and metallic plates, (T_{w1} and T_{w2}). Likewise, the air mass flow rate (m) is calculated. For this, five geometries (G_1, G_2, G_3, G_4, and G_5) are considered and different materials for the metal plates. Tables 1 and 2 describe the geometries and properties of the material.

3.2 Weather conditions

Solar irradiance, temperature, and airspeed are parameters considered for numerical simulations. These climatic conditions correspond to data for a whole year recorded in 2010 by a meteorological station located in Tlaquiltenango city in Morelos, Mexico. With latitude and longitude, 18 ° 68'33 "LN and -99 ° 11'67" LW, correspondingly. The Dickey-Fuller test was applied to examine the stationarity of the time series. The test confirms that the data are constant over time without a systematic increase or decrease in their values (Najid *et al.*, 2012). For example, the solar irradiance time series for the east (I_e) and west (I_o), orientation, and the air velocity (V) and air temperature (T_a) of two specific hours (12:00 and 15:00 hours) are shown in Figure 5.
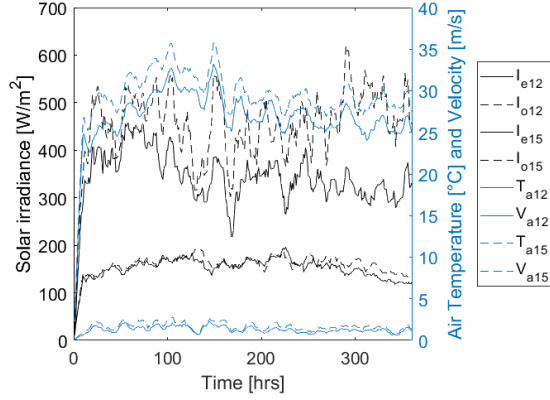
FIGURE 5. Solar irradiance on the east side ($I_{e_{15}}$ and $I_{e_{12}}$) and the west side ($I_{o_{15}}$ and $I_{o_{12}}$). Room temperature ($T_{a_{15}}$ and $T_{a_{12}}$) and speed ($V_{a_{15}}$ and $V_{a_{12}}$).

FIGURE 6. ANN architecture. Only a few connections represent fully interconnected neurons.

3.3 Artificial neural networks

Previously, artificial neural networks have been used to predict thermal phenomena applying the retro-propagation algorithm (Tlatelpa-Becerro, *et al.*, 2015; Reynoso-Jardón, *et al.*, 2019). The ANN architecture used in this predictive process consists of a hidden fully connected two-layer feedback ANN, trained by retro-propagation learning. The architecture has demonstrated its versatility to predict complex signals such as those involved in the transitory behavior of the solar chimney (Tlatelpa-Becerro, *et al.*, 2018).

There is no rigorous way to determine an optimal number of neurons in the hidden layer. The selection results from a compromise between the computational effort required for ANN training and an estimate of the minimum number of neurons necessary to capture dynamic behavior. Various network sizes are used to monitor the mean squared error (MSE, Equation 29) as an indicator of the training process performance. In addition, it uses conjugated gradient retro-propagation with Polak-Ribiere updates in the ANN training and validation process. The input vectors are normalized values between 0.1 and 0.9 due to the restriction of the sigmoid function [46] for the hidden and output layers (Krischer *et al.*, 1993). The transfer function and the normalization equation used are given by Equations 30 and 31, correspondingly.

The ANN architecture has four regular layers: twelve neurons in the input layer, two hidden layers with thirty-two neurons each, and eight neurons in the output layer (Figure 6). The input neurons correspond to the east solar irradiance orientation (I_e) and west
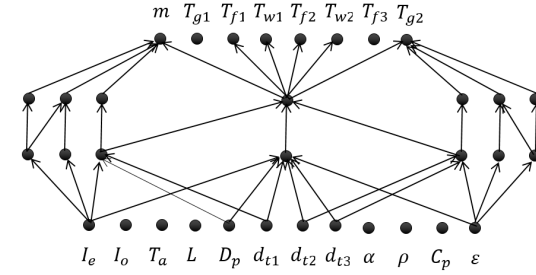
(I_o), air temperature (T_a), height (L), cavity widths (d_{t1}, d_{t2}, d_{t3}), density (ρ), specific heat (C_p). Finally, the absorptivity properties (α) and emissivity (ε). At the same time, the output neurons are the mass flow rate of air (m), glass cover temperatures (T_{g1}, T_{g2}), the temperatures of metal plates (T_{w1}, T_{w2}), and the temperatures of air currents (T_{f1}, T_{f2}, T_{f3}).

$$MSE = \sqrt{\frac{1}{Q}\sum_{q=1}^{Q}(z_q - a_q)^2} \qquad (29)$$

$$g(x) = \frac{[1 + \tanh(x)]}{2} \qquad (30)$$

$$X_i = 0.8\left(\frac{X_i - X_{\min}}{X_{\max} - X_{\min}}\right) + 0.1 \qquad (31)$$

4 Results

4.1 Numerical simulation results

The equations of the system (Equation 9) represent the temperature vector [T]. Section II describes how the heat transfer coefficients by convection and radiation the optical and physical properties of the materials are calculated for the proposed materials. Where $T_{g1,i}^{k+1}$ and $T_{g2,i}^{k+1}$ represent the temperatures of the glass cover, $T_{w1,i}^{k+1}$ and $T_{w2,i}^{k+1}$ temperature of the vertical metal plate, and $T_{f1,i}^{k+1}$, $T_{f2,i}^{k+1}$ and $T_{f3,i}^{k+1}$ air-fluid temperatures.

Two sets of simulations consider the calculation of temperatures and mass flow. The first simulation set considers four geometries (G_1, G_2, G_3 and G_4) and three materials (ductile steel, anodized aluminum, and copper with black smoke surfaces) for climatic conditions of the year 2010 for 15:00 hrs. Geometric dimensions and material properties are found in Tables 1 and 2.
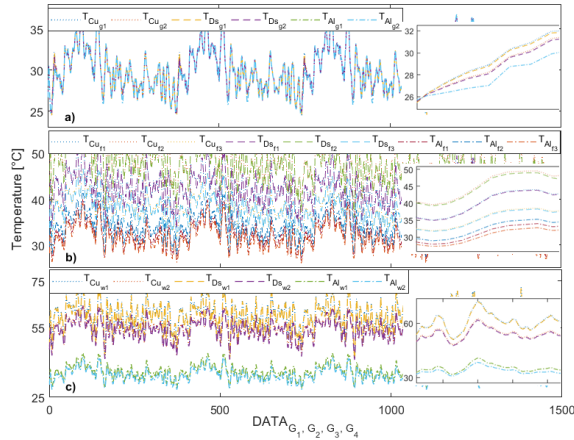
FIGURE 7. Temperatures time series of the solar chimney elements considering four geometries and three materials for the metal plate. a) Glass covers temperature. b) Air flows temperatures. c) Metal plates temperatures.
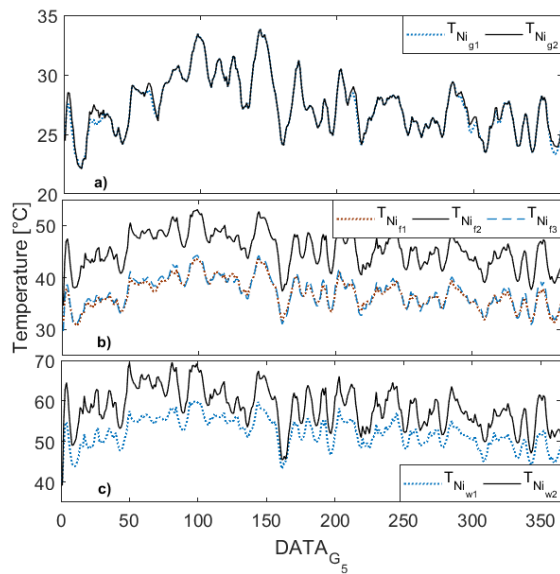

FIGURE 8. Temperatures Time Series of the Solar Chimney elements considering the geometry (G_5) and nickel oxide for the metal plate. a) Glass covers temperature. b) Air flows temperatures. c) Metal plates temperatures.

The glass cover temperatures (T_{g1} and T_{g2}) are shown in Figure 7 a). When using material such as copper ($T_{Cu_{g1}}$, $T_{Cu_{g2}}$), steel ($T_{Ds_{g1}}$, $T_{Ds_{g2}}$), and aluminum ($T_{Al_{g1}}$, $T_{Al_{g2}}$), the glass cover temperatures are between 25 to 35°C, maintaining an average of 30°C for most of the year. The temperature variation between the covers is 0 to 2°C. The air

temperatures results (T_{f1}, T_{f2}, T_{f3}) are located in the center of Figure 7 b). Here it is observed that the highest temperatures correspond to the air flow found in cavity 2, reaching an approximate average of 48°C of flow temperature when copper and ductile steel plates are used, being a little higher for copper. Whereas the average temperature when using aluminum plates is approximately 43 °C. The results of the metal plate temperatures (T_{w1} and T_{w2}) is shown at the bottom of Figure 7 c). The metal plate (T_{w1}) in the west orientation is that reaches the highest temperature. For this case. For this case, the copper plate temperature ($T_{Cu_{w1}}$) and steel ($T_{Ds_{w1}}$) is approximately 63 °C. While, in the east orientation, the metal plate temperature (T_{w2}), both for copper ($T_{Cu_{w2}}$) and steel ($T_{Ds_{w2}}$) is at 50 °C. When aluminum is used for metal plates temperatures ($T_{Al_{w1}}$) and $T_{Al_{w2}}$) are reached average about 35 °C, being the lowest among the other materials. The highest temperatures correspond to the west side, because there is more solar radiation.

The model was verified for a fifth geometry (G_5), considering nickel oxide in metal plates. Solar radiation, ambient temperature and air speed correspond to data obtained and recorded at noon that same year. The temperatures obtained from the numerical simulation for glass covers ($T_{Ni_{g1}}$, $T_{Ni_{g2}}$), air flows ($T_{Ni_{f1}}$, $T_{Ni_{f2}}$, $T_{Ni_{f3}}$) and metal plates ($T_{Ni_{w1}}$, $T_{Ni_{w2}}$) are shown in Figure 8.

Figure 9 shows the mass flow rate results for both sets of the numerical simulation. In sections a) and b), an increase in the mass flow rate is observed along the path; see figure 9. This trend is due to the type of geometry used, which the first section from left to right corresponds to G_1, followed by G_2, later G_3 and finally G_4. It is also appreciated that the mass flow rate m_{Cu} is slightly higher m_{Ds} with variations below 0.01 and 0.03 kg/s. That corresponds when metallic plates are used with copper and ductile steel.

This proximity between both flows is due to their material properties, which are very similar, copper with a black smoke surface being better. Both flows have an average magnitude of 1.2 kg/s, see Figure 9 a). However, the mass flow rate m_{Al} that corresponds when using metallic aluminum plates, the flow tends to be less than 50% compared to the others, this due to its optical and physical properties, Figure 9 b). While Figure 9 c) presents the results of the mass flow rate with an average of 0.5 kg/s when nickel oxide metal plates are used.
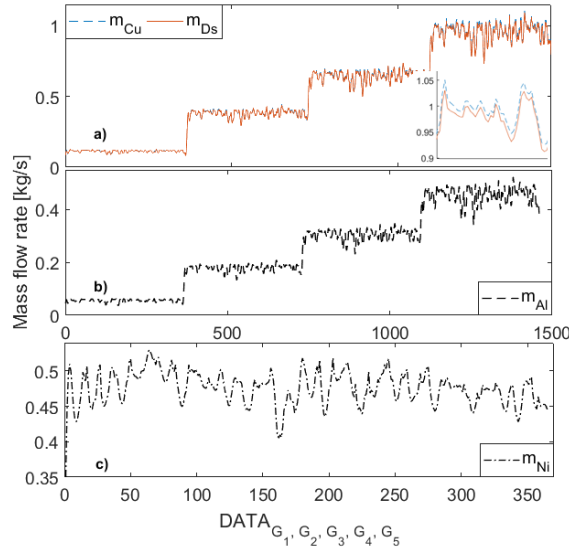
FIGURE 9. Air mass flow rate for nickel oxide material.

FIGURE 10. Comparison of predicted versus simulated element temperatures and mass flows. a) Glass covers temperature. b) Air flows temperature. c) Metal plates temperature and d) Mass flows.

The numerical simulations provide satisfactory results for the different geometries and materials, regardless of the climatic conditions, complying with the conditions of thermal comfort and air quality (Kohloss, 2004). However, suppose that the optimal design is required with a minimum investment cost (involving the definition of the geometry and the selection of the material). In that case, the process must be repeated for each geometry and material, with the consequent high computational cost. The remaining sections describe an alternative strategy to simplify this process, which involves building an ANN reference model.

4.2 ANN results

The ANN architecture has four regular layers: twelve neurons in the input layer, two hidden layers with thirty-two neurons each, and eight neurons in the output layer for model verification and validation. One third of the data set when using the materials steel, copper and aluminum were used to test the dynamic response of the system. The validation of the predictive model was executed with a set of 365 data for the use of the nickel material.

Figure 10 shows the results of the prediction of temperatures and mass flows of the solar chimney. For example, heading (a) shows the predicted glass cover temperatures ($T_{G1_{ANN}}$, $T_{G2_{ANN}}$) closely following the simulated ($T_{G1_{sim}}$, $T_{G2_{sim}}$), with a deviation ($RE_{T_{G1}}$, $RE_{T_{G2}}$), below 0.1%, Figure 11 a).

FIGURE 11. Relative Error Comparison between the predicted and simulated temperatures and mass flows. a) Relative error between glass covers. b) Relative error between air flows. c) Relative error between metal plates and d) Relative error of the mass flow rate.

Heading (b) shows the results for air temperatures ($T_{f1_{ANN}}$, $T_{f2_{ANN}}$, $T_{f3_{ANN}}$) versus simulated temperatures ($T_{f1_{sim}}$, $T_{f2_{sim}}$, $T_{f3_{sim}}$) for cavities C_{t1},
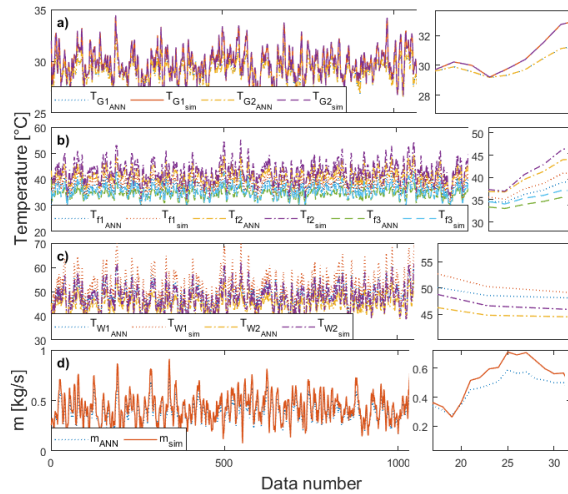
FIGURE 12. Comparison of predicted versus simulated element temperatures and mass flows rate. a) Glass covers temperature. b) Air flows temperature. c) Metal plates temperature and d) Mass flows rate.
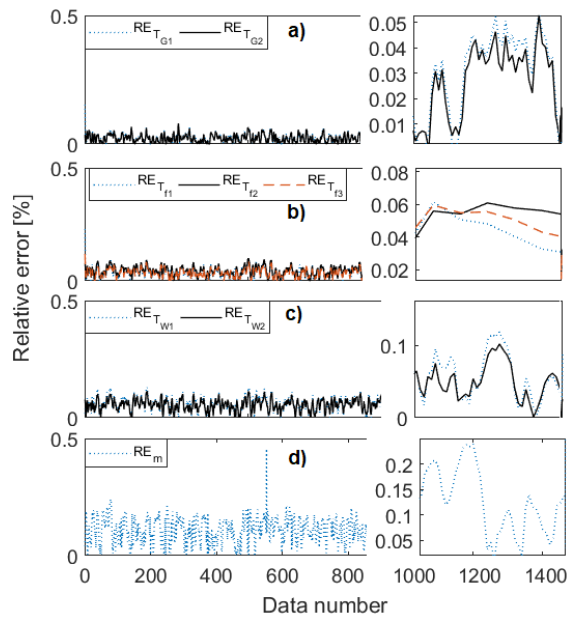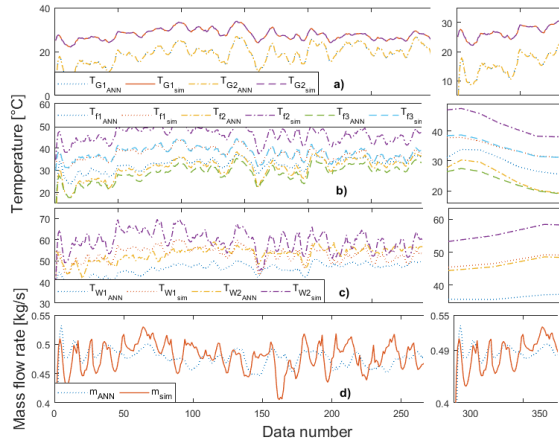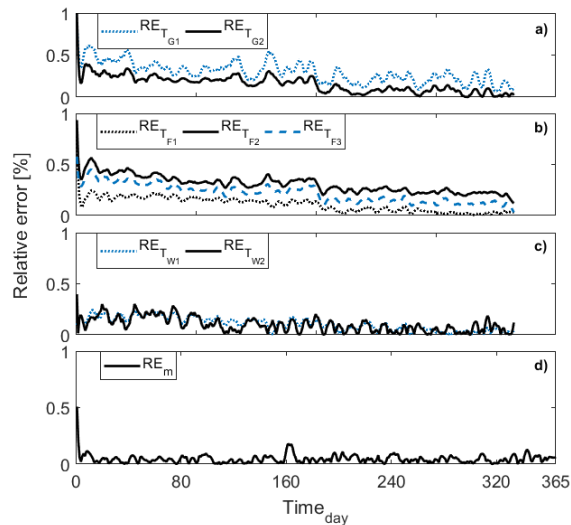

FIGURE 13. Relative Error Comparison between the predicted and simulated temperatures and mass flows rate. a) Relative error between glass covers. b) Relative error between air flows. c) Relative error between metal plates and d) Relative error of the mass flow rate.

C_{t2}, C_{t3}. Although higher temperatures are observed between metal plates (C_{t2}), this is due to the exchange of energy. While the lowest temperature is in the cavity C_{t3}. The temperatures predictions of the flows through the network match the simulated data with a deviation (RE_{Tf1}, RE_{Tf2}, RE_{Tf3}) below 0.12%, Figure 11 b). Similarly, the prediction of the temperatures of the metal plates ($T_{W1_{ANN}}$, $T_{W2_{ANN}}$) closely follow the trajectory of simulated temperatures ($T_{W1_{sim}}$, $T_{W2_{sim}}$),

Figure 10 c). The error (RE_{TW1}, RE_{TW2}) between both results is below 0.12%, Figure 11 c). While heading d) shows the predicted mass flow rate (m_{ANN}) versus simulated (m_{sim}), which presents a maximum variation of 0 to 0.1 kg/s throughout the trajectory with a relative error (RE_m) below 0.3%, Figure 10 d).

The ANN predictions are validated using a second data set from the simulations involving oxidized nickel as the reference material and the geometry. G_5, Table 1 and 2. The meteorological conditions used correspond to noon of the same year. The deviation between predicted and simulated data for glass covers, airflow, and metal plate temperatures is below 0.7, 0.5, and 0.3%, respectively (Figure 13). With these results, we can indicate that the ANN reference model can extrapolate the predictions of the chimney behavior for materials and geometries not considered during the training process.

Conclusions

An ANN reference model strategy has been described to simulate the behavior of solar chimneys for different materials and geometries. This model uses for its generation of chimney configuration simulations under other climatic conditions, materials, and geometries. The ANN model shows excellent results in predicting mass flow rate and internal temperature variations. The method can become a valuable tool to optimize configuration and reduce investment and operating costs. This description must be complemented with an estimate of the life cycles of the materials associated with the phenomena of corrosion, operating expenses, and deterioration of the operating efficiency due to depositions and encrustations that can deteriorate the functioning of the chimney, and that should be included in a complete estimate of the investment for its installation.

For the case studied, the best chimney performance is achieved with copper due to the more efficient energy transport. Copper, however, is frequently noted as prone to corrosive effects, so in a broader perspective, other materials that, although exhibit worse performance, are more resistant to corrosion, such as aluminum, must be considered.

Alloys and other materials such as steel can present an even better compromise when considering the running costs and life cycle of the Chimneys. Thus, the proposed strategy becomes increasingly important in this process, allowing to test of a

more significant number of materials, geometries, and climatic conditions in a simple and economical way (in time and computational costs).

The strategy entails obtaining a "general and robust" predictor, necessary to be considered as an optimal design tool for the selection of materials and geometry of solar chimneys. However, it must be taken into account that other factors, such as extreme weather conditions, high temperatures, and humidity, can affect the performance of the chimney and should be considered part of the evaluation (Kuźnicka, 2009; Usman and Nusair, 2008; Ranjbar, 2010). In future contributions, we will explore these additional aspects of the solar chimney design.

The strategy entails obtaining a "general and robust" predictor, necessary to be considered an optimal design tool for selecting materials and geometry of solar chimneys. However, it must be taken into account that other factors, such as extreme weather conditions, high temperatures, and humidity, can affect the chimney's performance and should be considered part of the evaluation (Kuźnicka, 2009; Usman and Nusair, 2008; Ranjbar, 2010). We will explore these additional aspects of the solar chimney design in future contributions.

Nomenclature

A_r	Aspect ratio of the area (A_o/A_i)
A_o	Outlet area (m^2)
A_i	Inlet area (m^2)
$C_{t1,2,3}$	Airflow cavities
C_p	Specific Heat of the materials (J/kgK)
C_p	Specific Heat of the materials (J/kgK)
$C_{f1,2,3}$	Specific Heat of the fluid (J/kgK)
C_d	Discharge coefficient (geometry)
$d_{t1,2,3}$	Width each cavity of the chimney (m)
D_p	Depth of the chimney (m)
D_h	Hydraulic diameter (m)
$\dot{E}_{st}$	Stored thermal and mechanical energy
$\dot{E}_{out}$	Output mechanical and thermal energy transport through control surfaces
$\dot{E}_{in}$	Input mechanical and thermal energy transport through control surfaces
$\dot{E}_g$	Thermal energy generation
G_{c1}, G_{c2}	Glass covers
$G_{1,2,3,4,5}$	Geometry
$g(x)$	Transfer function
h_{wind}	Convective wind coefficient (W/(m^2 K))
$h_{w11,22}$	Convective heat transfer coefficient between metal plate and air cavity (W/(m^2 K))

$h_{w1,2}$	Convective heat transfer coefficient between metal plate and air cavity (W/(m^2 K))
$h_{g1,2}$	Convective heat transfer coefficient between glass cover and air cavity (W/(m^2 K))
$h_{rww1,2}$	Radiative heat transfer coefficient between metal plates (W/(m^2 K))
$h_{rwg1,2}$	Radiative heat transfer coefficient between metallic and glass cover(W/(m^2 K))
h_{rs}	Radiative heat transfer coefficient between glass cover and sky (W/(m^2 K))
I_o	Solar irradiance for the west orientation (W/m^2)
I_e	Solar irradiance for the east orientation (W/m^2)
L	Length of the chimney (m)
m	Air mass flow rate (kg/s)
M	Relationship between mass flow rate, specific heat and chimney geometry
MSE	Mean squared error (%)
$P_{m1,2}$	Vertical metal plates
$q_{1,2,3}$	Heat flux (W/m^2)
Re_D	Reynolds number
RE_m	Relative error of air mass flow rate (%)
$RE_{T_f1,2,3}$	Relative error of the fluid (%)
$RE_{T_{W1,2}}$	Relative error of metal plate (%)
$RE_{T_{G1,2}}$	Relative error of glass cover (%)
$S_{w1,2}$	Solar radiation heat flux absorbed by the metal plate (W/m^2)
$S_{g1,2}$	Solar radiation heat flux absorbed by the glass cover(W/m^2)
$T_{w1,2}$	Metal plate Temperature (°C)
$T_{w1,2,i}^{k+1}$	Metal plate temperature by numerical simulation to one step (°C)
T_{sky}	Sky temperature (°C)
$T_{g1,2}$	Glass cover temperature (°C)
$T_{g1,2,i}^{k+1}$	Glass cover temperatures by numerical simulation to one step (°C)
$T_{f1,2,3}$	Airflow temperature (°C)
$T_{f1,2,3,i}^{k+1}$	Airflow temperature by numerical simulation to one step (°C)
T_a	Ambient temperature (°C)
$T_{G1,2sim}$	Glass cover temperature calculated by numerical simulation (°C)
$T_{G1,2ANN}$	Glass cover temperature predicted by ANN (°C)
$T_{f1,2,3sim}$	Airflow temperature calculated by numerical simulation (°C)
$T_{f1,2,3ANN}$	Airflow temperature predicted by ANN (°C)

$T_{W1,2_{sim}}$	Metal plate temperature calculated by numerical simulation (°C)
$T_{W1,2_{ANN}}$	Metal plate temperature predicted by ANN (°C)
$T_{Ni_{w1,2}}$	Nickel metal plate temperature calculated by numerical simulation (°C)
$T_{Ni_{g1,2}}$	Nickel glass cover temperature calculated by numerical simulation (°C)
$T_{Ni_{f1,2,3}}$	Nickel airflow temperature calculated by numerical simulation (°C)
$T_{Ds_{w1,2}}$	Ductile steel metal plate temperature calculated by numerical simulation (°C)
$T_{Ds_{g1,2}}$	Glass cover temperature by numerical simulation with ductile steel material (°C)
$T_{Cu_{w1,2}}$	Copper metal plate temperature calculated by numerical simulation (°C)
$T_{Cu_{g1,2}}$	Glass cover temperature by numerical simulation with copper material (°C)
$T_{Al_{w1,2}}$	Aluminum metal plate temperature calculated by numerical simulation (°C)
$T_{Al_{g1,2}}$	Glass cover temperature by numerical simulation with aluminum material (°C)
$U_{t1,2}$	Overall heat transfer coefficient from top of glass cover (W/(m^2 K))
V	Wind velocity (m/s)
W	Full width of the chimney (m)
w	Width of the chimney (m), considering the sum of the three cavities ($d_{t1} + d_{t2} + d_{t3}$)
X_{min}	Minimum value
X_{max}	Maximum value
X_i	Value to normalize
Greek Symbols	
ρ	Density (kg/m^3)
β	Ratio of the flow through the width chimney
τ	Transmissivity
α	Absorptivity
ε	Emissivity
μ	Dynamic viscosity (kg/ms)
Subscripts	
f	Fluid
g	Glass
i	Section number (i = 1, 2, … n)
sim	Simulation
Ds	Ductile Steel
Cu	Copper
Al	Aluminum
Ni	Nickel
ANN	Artificial neural networks

References

Akbari, S., Simonson, C.J. and Besant, R.W. (2012). Application of neural networks to predict the transient performance of a run-around membrane energy exchanger for yearly non-stop operation. *International Journal of Heat and Mass Transfer 55*(21-22), 5403-5416. https://doi.org/10.1016/j.ijheatmasstransfer.2012.04.033

Akdag, U., Komur, M.A. and Ozguc, A.F. (2009). Estimation of heat transfer in oscillating annular flow using artifical neural networks. *Advances in Engineering Software 40*(9), 864-870. https://doi.org/10.1016/j.advengsoft.2009.01.010

Awbi, H. B. (1994). Design considerations for naturally ventilated buildings. *Renewable Energy 5*(5-8), 1081-1090. https://doi.org/10.1016/0960-1481(94)90135-X

Bansal, N.K., Mathur, J., Mathur, S. and Jain, M. (2005). Modeling of window-sized solar chimneys for ventilation. *Building and Environment 40*(10), 1302-1308. https://doi.org/10.1016/j.buildenv.2004.10.011

Bansal, N.K., Mathur, R. and Bhandari, M.S. (1994). A study of solar chimney assisted wind tower system for natural ventilation on buildings. *Building and Environment 29*(4), 495-500. https://doi.org/10.1016/0360-1323(94)90008-6

Beigzadeh, R. and Rahimi, M. (2012). Prediction of heat transfer and flow characteristics in helically coiled tubes using artificial neural networks. *International Communications in Heat and Mass Transfer 39*(8), 1279-1285. https://doi.org/10.1016/j.icheatmasstransfer.2012.06.008

Brusamarello, C., Di Domenico, M., Da Silva, C., and de Castilhos, F. (2019). A comparative study between multivariate calibration and artificial neural network in quantification of soybean biodiesel. *Revista Mexicana de Ingeniería Química 19*(1), 123-132. https://doi.org/10.24275/rmiq/Bio579

Cengel, Y. and Boles, M. (2015). *Thermodynamics*. McGraw-Hill Education, México.

Chantawong, P., Hirunlabh, J., Zeghmati, B., Khedari, J., Teekasap, S. and Win, M.M. (2006). Investigation on thermal performance of glazed solar chimney walls. *Solar Energy 80*(3), 288-297. https://doi.org/10.1016/j.solener.2005.02.015

Díaz, G,, Sen, M., Yang, K. T. and McClain, R.L. (2001). Dynamic prediction and control of heat exchangers using artificial neural networks. *International Journal of Heat and Mass Transfer 44*(9), 1671-1679. https://doi.org/10.1016/S0017-9310(00)00228-3

Díaz-González, L., Hidalgo-Davila, C., Santoyo, E. and Hermosillo-Valadez, J. (2020). Evaluation of training techniques of artificial neural networks for geothermometric studies of geothermal systems. *Revista Mexicana de Ingeniería Química 12*(1), 105-120. http://www.rmiq.org/ojs311/index.php/rmiq/article/view/1462

Duffie, J.A., Beckman, W.A. and McGowan, J. (1985). *Solar Engineering of Thermal Processes*. John Wiley & Sons, Inc, Canada.

Esen, H. and Inalli, M. (2009). Modelling of a vertical ground coupled heat pump system by using artificial neural networks. *Expert Systems with Applications 36*(7), 10229-10238. https://doi.org/10.1016/j.eswa.2009.01.055

González, G.R., Rico, M.R. and Kevrekidis, I. G. (1998). Identification of distributed parameter systems: a neural net based approach. *Computers and Chemical Engineering 22*, 965-968. https://doi.org/10.1016/S0098-1354(98)00191-4

Hirunlabh, J., Kongduang, W., Namprakai, P. and Khedari, J. (1999). Study of natural ventilation of houses by a metallic solar wall under tropical climate. *Renewable Energy 18*(1), 109-119. https://doi.org/10.1016/S0960-1481(98)00783-6

Imran, A.A., Jalil, J.M. and Ahmed, S.T. (2015). Induced flow for ventilation and cooling by a solar chimney. *Renewable Energy 78*, 236-244. https://doi.org/10.1016/j.renene.2015.01.019

Incropera, F.P. and DeWitt, D.P. (1999). *Fundamentals of Heat Transfer*. Pearson Education, México.

Islamoglu, Y. (2003). A new approach for the prediction of the heat transfer rate of the wire-on-tube type heat exchanger-use of an artificial neural network model. *Applied Thermal Engineering 23*(2), 243-249. https://doi.org/10.1016/S1359-4311(02)00155-2

Karima, E.A. and Saif, W.M. (2012). Experimental and numerical studies of solar chimney for natural ventilation in Iraq. *Energy and Buildings 47*, 450-57. https://doi.org/10.1016/j.enbuild.2011.12.014

Khedari, J., Kaewruang, S., Pratinthong, N. and Hirunlabh, J. (1999). Natural ventilation of houses by a trombe wall under the climatic conditions in Thailand. *International Journal of Ambient Energy 20*(2), pp. 85-94. https://doi.org/10.1080/01430750.1999.9675323

Kohloss, F.H. (2004). ASHRAE for standard ventilation for acceptable air quality. *ANSI/ASHRAE Addendum n to ANSI/ASHRAE Standard 62-2001*, 8400.

Krischer, K., Rico, M.R., Kevrekidis, G., Rotermund, H.H., Ertl, G., and Hudson, J.L. (1993). Model identification of a spatiotemporally varying catalytic reaction. *AIChE Journal 39*(1), 89-98. https://doi.org/10.1002/aic.690390110

Kuźnicka, B. (2009). Erosion-corrosion of heat exchanger tubes. *Engineering Failure Analysis 16*(7), 2382-2387. https://doi.org/10.1016/j.engfailanal.2009.03.026

Layeni, A.T., Adekojo, W.M., Babatunde, A.A., Bukola, O.B., Collins, N.N. and Solomon, O.G. (2020). Computational modelling and simulation of the feasibility of a novel dual purpose solar chimney for power generation and passive ventilation in buildings. *Scientific African 8*, 1-13. https://doi.org/10.1016/j.sciaf.2020.e00298

Li, W., Yu, G., Zagaglia, D., Green, R. and Yu, Z. (2020). CFD Modelling of a thermal chimney for air-cooled condenser. *Geothermics 88*, 1-19. https://doi.org/10.1016/j.geothermics.2020.101908

Najid, A., Hayat, M.F., Hamad, N. and Iuqman, M. (2012). Energy consumption and economic growth: evidence from Pakistan. *Australian Journal of Business and Management Research 2*(6), 49-53. https://doi.org/10.1002/mde.4090050108

Oliva, A.I., Maldonado, R.D., Díaz, E. A. and Montalvo, A.I. (2013). A high absorbance material for solar collectors' applications. Third Congress On Materials Science And Engineering (CNCIM-Mexico 2012). *IOP Conference Series: Materials Science and Engineering 45*(1), 2-6. doi.org/10.1088/1757-899X/45/1/012019

Patel, S.K., Prasad, D. and Ahmed, R.M. (2014). Computational studies on the effect of geometric parameters on the performance of a solar chimney power plant. *Energy Conversion and Management 77*, 424-431. https://doi.org/10.1016/j.enconman.2013.09.056

Peng, H. and Ling, X. (2009). Neural networks analysis of thermal characteristics on plate-fin heat exchangers with limited experimental data. *Applied Thermal Engineering 29*(11-12), 2251-2256. https://doi.org/10.1016/j.applthermaleng.2008.11.011

Ramadan, B. and Nader S.A. (2008). An analytical and numerical study of solar chimney use for room natural ventilation. *Energy and Buildings 40*(5), 865-873. https://doi.org/10.1016/j.enbuild.2007.06.005

Ramadan, B. and Nader S.A. (2009). Effect of solar chimney inclination angle on space flow pattern and ventilation rate. *Energy and Buildings 41*(2), 190-196. https://doi.org/10.1016/j.enbuild.2008.08.009

Ranjbar, K. (2010). Effect of flow induced corrosion and erosion on failure of a tubular heat exchanger. *Materials and Design 31*(1), 613-619. https://doi.org/10.1016/j.matdes.2009.06.025

Reynoso-Jardón, E., Tlatelpa-Becerro, A., Rico-Martínez, R., Calderón-Ramírez, M. and Urquiza, G. (2019). Artificial neural networks (ANN) to predict overall heat transfer coefficient and pressure drop on a simulated heat exchanger. *International Journal of Applied Engineering Research 14*(13), 3097-3103.

Saifi, N., Settou, N., Dokkar, B., Negrou, B. and Chennouf, N. (2012). Experimental study and simulation of airflow in solar chimneys. *Energy Procedia 18*, 1289-1298. https://doi.org/10.1016/j.egypro.2012.05.146

Sakonidou, E.P., Karapantsios, T.D., Balouktsis, A.I. and Chassapis, D. (2008). Modeling of the optimum tilt of a solar chimney for maximum air flow. *Solar Energy 82*(1), 80-94. https://doi.org/10.1016/j.solener.2007.03.001

Shi, L. and Zhang, G. (2016). An empirical model to predict the performance of typical solar chimneys considering both room and cavity configurations. *Buildings and Environment 103*, 250-261. https://doi.org/10.1016/j.buildenv.2016.04.024

Sudprasert, S., Chinsorranant, Ch. and Rattanadecho, P. (2016). Numerical study of vertical solar chimneys with moist air in a hot and humid climate. *International Journal of Heat and Mass Transfer 102*, 645-656. https://doi.org/10.1016/j.ijheatmasstransfer.2016.06.054

Tlatelpa-Becerro, A., Castro-Gómez, L., Urquiza, G. and Rico-Martínez, R. (2015). Prediction of the outlet temperature of an experimental heat exchanger using artificial neural networks. *Computational Methods and Experimental Measurements XVII 1*(2015), 213-220. https://doi.org/10.2495/cmem150191

Tlatelpa-Becerro, A., Rico-Martínez, R., Castro-Gómez, L., Urquiza, G. and Calderón-Ramírez, M. (2018). Artificial neural networks (ann) and kalman filter algorithms to predict output temperatures on a heat exchanger. *International Journal of Applied Engineering Research 13*(17), 13130-13135.

Usman, A. and Nusair, A.K. (2008). Failure analysis of heat exchanger tubes. *Engineering Failure Analysis 15*(1-2), 118-128. https://doi.org/10.1016/j.engfailanal.2006.11.051

White, F.M. (2004). *Fluid Mechanics*. McGraw-Hill, Inc, Madrid.

Xie, G. N., Wang, Q. W., Zeng, M. and Luo, L. Q. (2007). Heat transfer analysis for shell-and-tube heat exchangers with experimental data by artificial neural networks

approach. *Applied Thermal Engineering 27*(5-6), 1096-1104. https://doi.org/10.1016/j.applthermaleng.2006.07.036

Xie, G., Sunden, B., Wang, Q. and Tang, T. (2009). Performance predictions of laminar and turbulent heat transfer and fluid flow of heat exchangers having large tube-diameter and large tube-row by artificial neural networks. *International Journal of Heat and Mass Transfer 52*(11-12), 2484-2497. https://doi.org/10.1016/j.ijheatmasstransfer.2008.10.036

Zhang, J. and Haghighat, F. (2010). Development of artificial neural network based heat convection algorithm for thermal simulation of large rectangular cross-sectional area earth-to-air heat exchangers. *Energy and Buildings 42*(4), 435-440. https://doi.org/10.1016/j.enbuild.2009.10.011

Zhongbao, L. and Su, Y. (2012). An unsteady model for natural ventilation with solar chimney. *Advanced Materials Research 354-355*, 286-289. https://doi.org/10.4028/www.scientific.net/AMR.354-355.286